

Analysis of Age and Metallicity of Stellar Cluster M3 and M67

Anthony Lazos¹, Atirath Dhara², and JT Earwicker³

^{1,2,3}Astronomy Advanced Lab 135, Prof Olivier Hervet and TA Miguel Escobar Godoy

May 2023

1 Abstract

In this study, we observed the stellar clusters Messier 3(M3) and Messier 67(M67) on April 13th, 2023 with the Nickel Telescope at the Lick Observatory. Our analysis utilizes source extractor to obtain stars' fluxes which we convert to magnitudes to ultimately create Hertzsprung-Russell diagrams. We then fit these with theoretical isochrones to determine the ages and metallicities of the clusters. We found M3 to be between 11.22 Gyr and 15.85 Gyr and $Z = 0.001$ and M67 to be between 3.55 Gyr and 4.49 Gyr and $Z = 0.019$. These results agree well with other values found in current literature.

2 Introduction

Globular clusters are roughly spherical groups containing thousands to millions of stars all within only a few parsecs of their neighbors. These clusters are very old between, 10 and 13 billion years, and contain a very low percentage of metals, mostly consisting of hydrogen and helium. Open clusters are groups of only tens to a few hundred stars and are much less dense. These clusters are much younger than globular clusters and range from a few million years to about 8 billion years. Due to their relatively young age, there were more metals in the galactic dust that these stars formed from, so they have a higher percentage of heavier elements within them.

In this paper, we will focus on the globular cluster Messier 3(M3) and the open cluster Messier 67(M67). M3 is located approximately 9.09kpc [1] from Earth and contains 100,000 stars [2]. M67 is located at 883pc [3] from Earth and is interesting because it is a very old open cluster, estimated to be 3-4.5 billion years [4]. In this study, we seek to determine the ages and metallicity of M3 and M67. This will be done by creating a Hertzsprung-Russell diagram for each cluster, which plots absolute magnitude in a filter vs difference of magnitudes of two filter that correspond to temperature, and fitting isochrones of various ages and metallicities to find one that provides a good fit for our data.

The sections that follow will describe the observation procedure, explain the analysis process, present our results, and discuss and compare our results with other work done with these clusters.

3 Observation

We took observations on Thursday, April 13th, 2023 from the Lick Observatory using the Nickel telescope which is a 1-meter reflecting telescope with a CCD capable of observing from the near-ultraviolet to the near-infrared [5]. We used three filters blue(B) at 432.6 nm, green(V) at 532.4 nm, and red(R) at 624.3 nm. These wavelengths were found by calculating the full-width-half-maximum of transmission percentages for each of the filters provided by the Lick Observatory [6].

We calibrated Nickel by first taking 10 biases, then 5 flats with each filter using the dome's light. When it became dark enough, we focused our camera by taking multiple images of the same standard star at multiple focus settings. Then, we compared these images by eye and chose the focus that provided the sharpest image of the star. This is the setting we used for our further observations.

We then began observations with our calibration star, the hot sub-dwarf PG 0918+029. Afterwards we moved on to our main targets: M3 then M67. The locations in global coordinates, observing time in Pacific Daylight Time(PDT), exposure time in seconds for each filter, and number of exposures taken for each filter are given in table 1. The weather was clear throughout the night of all these observations and caused no interruptions.

Source	Time(PDT)	Location(RA, Dec)	Airmass	Exposure(s)(B, V, R)	Images(B, V, R)
Bias	-	-	-	0	10
Dome Flats	-	-	-	45, 10, 3	5, 5, 5
PG 0918+029	21:30-21:40	09:21:28.21, +02° 46' 02.25"	1.22	80 ,80, 120	5, 5, 5
M3	21:45-22:15	13:42:11.62, +28° 22' 38.2"	1.04	250, 250, 150	3, 3, 5
M67	00:05-00:35	08:51:23.0, +11° 48' 502"	1.29	120, 60, 60	5, 5, 5

Table 1: Details of our observations. Location is given in global coordinates. Time in Pacific Daylight Time. Airmass is number of airmasses when looking at our source. Exposure is in seconds for each filter. The length was determined though trial and error until we found a length that would give us significant detection without getting close to saturating our camera. Lastly, the number of images per filter. The bias doesn't require a filter so the same images are used for all filters.

4 Data Processing

4.1 Image Cleaning

The first step in data processing was to convert the raw data into a usable science image. For this we needed a single master flat for each filter and a master bias. These steps are as follows:

1. Remove the rightmost 32 columns from the image. They were covered on the camera and provided no data on the clusters.
2. Take the median of the related images, pixel by pixel. This removes cosmic rays from the images.
3. Remove dead pixels by taking the average of their neighbors.

The files we have now are 1 master bias and 3 master flats, one for each filter. We used these to get our science images thorough the following process:

1. Remove the rightmost 32 columns from the image.
2. Get a clean flat by subtracting the master bias from the master flat. This removes background noise from the detector from our flat images.
3. Normalize the clean flat by dividing the clean flat by the average pixel value of the flat. This scales the pixels' sensitivities so that they all have a uniform response to light.
4. Get a clean science image by subtracting the master bias from the science data. Again, this removes background noise due to the detector.
5. Get the flux per second by dividing the clean science image by the corresponding exposure time. Flux per second is more useful because longer exposure will have larger fluxes, but we expect flux per second to be independent of exposure times.
6. For each filter, get a master science image by taking the median of the respective filters. This, again, removes cosmic rays.
7. Get a calibrated science image by dividing each master science image by the normalized flat. This removes the variations in sensitivity so that each pixel in our final image has the same sensitivity to light.

8. Finally we remove the dead pixels by taking the average of their neighbors.

With that we have nine calibrated science images shown in figure 1.

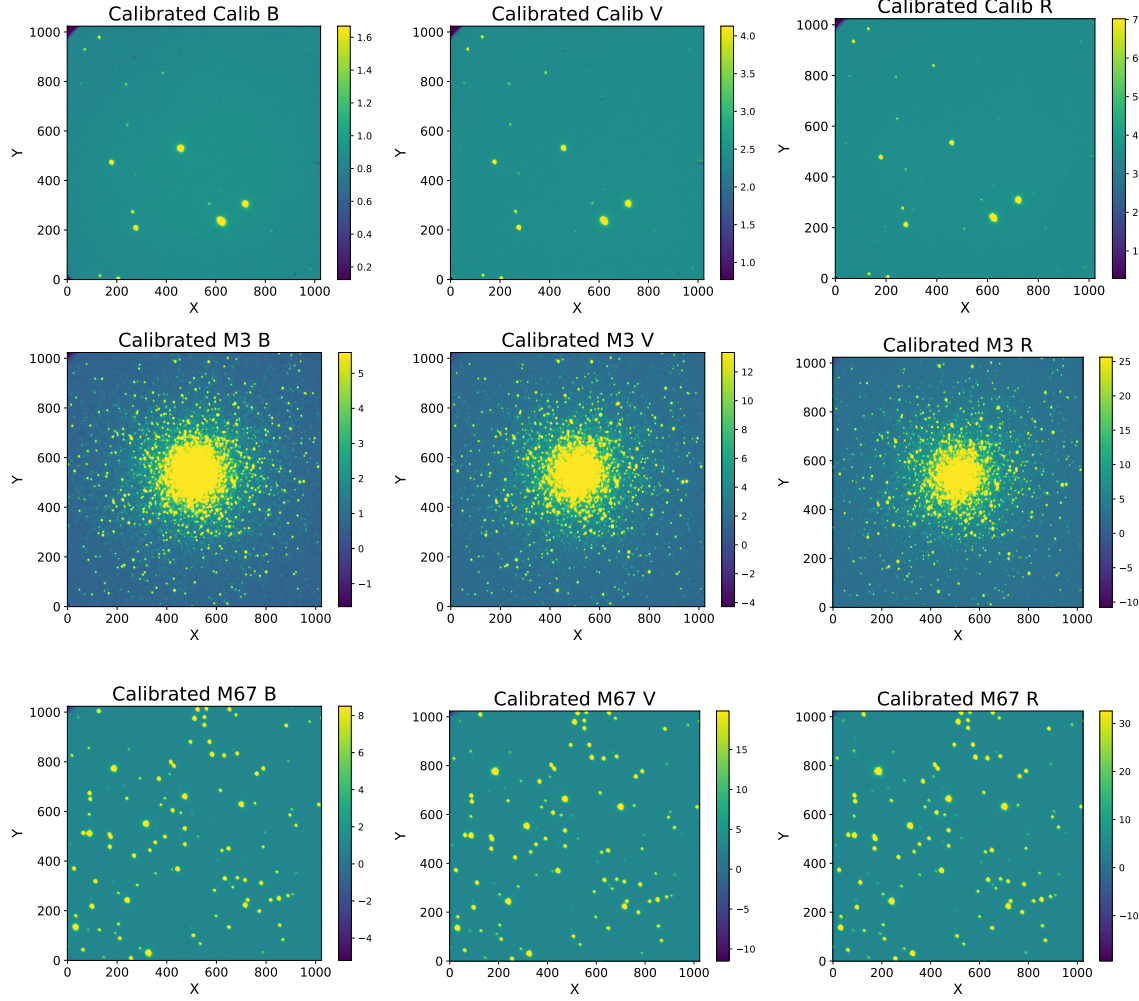


Figure 1: The cleaned science images for each source-filter combo. The first row is the calibration star PG 0918+029, the second row is M3, and the third row is M67. Note that the color bar scale is different for each image which corresponds to the various intensities between each source and filter.

4.2 Photometry

With the calibrated science images, we could then extract data from our clusters using the sep python package [7] for access to source extractor. The process for each image is:

1. Use `sep.background()` to calculate background noise. We will refer to this file as `bgk` (background).
2. Subtract the background from the calibrated science image. This removes noise from our image. We will refer to this file as `bgkrm` (background removed).
3. Use `sep.extract(data=bgkrm, thresh=2, err=bkg.globalrms)` to get a list of objects detected in the image. The choice of a thresh of 2 was simply through testing to see what extracted a decent number of stars. Examples of all our original objects detected are shown on the left in figure 2.

4. Create criterion to select only single stars that we can use. The criterion that we used were
 - a) PG 0918+029: Check the position of the star using Aladin Sky Atlas by comparing its location with that of near by stars. Then only take the star that has this one's exact coordinates because it is the only one we want.
 - b) M3: Both the x and y spread was less than 44 pixels, the difference between semi-major and semi-minor lengths were less than 2 pixels, and that the second detection was no further than 22 pixels.
 - c) M67: Contained least 100 pixels and the difference between the semi-minor and semi-major axis was less than 2 pixels.

This criterion helped to remove large groups and many pairs of stars.

5. Use `sep.sum_circle(data=bkgrm, x, y, radius, err=bkg.globalrms, gain=1.0)` to obtain fluxes and flux errors. We used radii of 35 pixels for PG 0918+029, 22 pixels for M67 and 8 pixels for M3 Figure 2 shows exactly what areas flux was calculated from after applying the filtering process and radii that `sum_circle` used.

At this point we had fluxes from our stars and were ready to calculate their magnitudes.

4.3 Calculating Magnitude

Before calculating magnitudes we must define our variables:

1. The zero point magnitude, m_{zp} .
2. The apparent magnitude of filter I, m_I .
3. The flux, N
4. The atmospheric extinction $m_{ext,atm}$.
5. The galactic dust extinction $m_{ext,dust}$
6. The parallax of our sources in mili-arcseconds, mas
7. The distance of our sources in parsecs, d

Most of this is clearly layed out in table 2.

Extinctions are the magnitudes of light absorbed in each wavelength due to either the atmosphere of Earth or the dust between Earth and our source. Atmospheric extinction was calculated by using the filters' wavelengths to interpolate the specific extinction per airmass for the source from Lick's Mean Extinction table [8]. Then we multiplied the airmass of our source by the extinction we found to get the atmospheric extinction for that source. The dust extinction was done by finding the extinction for a wavelength of 550nm using the GalExtin database [9] and the Amôres Lepine model [10] with galactic coordinates from Simbad [11] and distances in kiloparsecs converted from parallax in mili-arcseconds for PG 0918+029 [12], M3 [1], and M67 [3]. Then we used code provided to us by our instructor, Olivier Hervet [13], to convert the 550 nm extinction provided from GalExtin to the appropriate extinction for our three filters. Finally, we multiplied the 550 nm extinction by the factor needed to reach the correct wavelength and thus obtain the correct dust extinction. These extinctions are shown in table 2.

The process for calculating magnitudes is as follows:

1. Calculate the zero point magnitude using equation 1. We obtained the apparent magnitudes for PG 0918+029 from Landolt [8].
2. Calculate the apparent magnitude for each star using equation 2.
3. Calculate the distance to each cluster using equation 3.

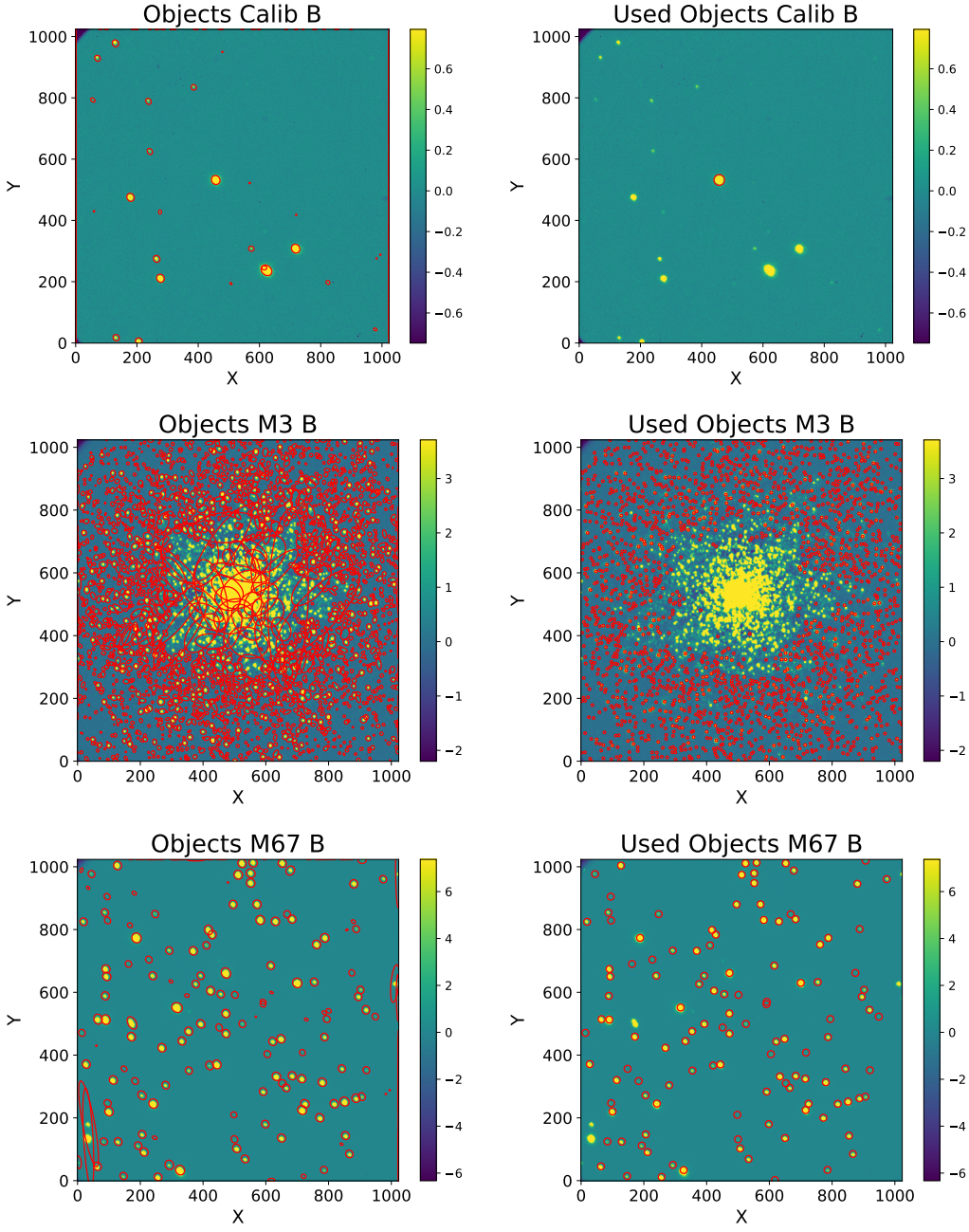


Figure 2: On the left are all the objects source extractor picked out originally. On the right is what stars we are using the flux from and the corresponding area after applying the filter conditions and selecting the appropriate radii for each source. Here we show the B filter only as an example, but, of course, the same was applied to the other filters.

Source	Distance(pc)	Filter	Atmosphere	Dust	Flux	Zero Point Magnitude
PG 0918+029		B	0.378	0.192	23.16± 0.01	6509.00 ± 80.78
		V	0.227	0.154	23.14± 0.01	5926.42± 77.17
		R	0.174	0.128	23.25± 0.01	62.83.96± 79.42
M3	9090	B	0.321	0.108	-	↓
		V	0.192	0.086	-	↓
		R	0.147	0.072	-	↓
M67	883	B	0.398	0.214	-	↓
		V	0.238	0.172	-	↓
		R	0.183	0.142	-	↓

Table 2: A summary of the necessary information for computing absolute magnitudes. The atmosphere and dust columns are the extinction values. Flux is only provided for the calibration star because we are only looking at a single star and not 100s of them like in the clusters. The zero point magnitude is calculated using the calibration star but is used again in the magnitude calculations for M3 and M67.

4. Calculate absolute magnitude we use equation 4

$$m_{zp} = m_I + 2.5\log_{10}(N) + m_{ext,atm} + m_{ext,dust} \quad (1)$$

$$m_I = -2.5\log_{10}(N) - m_{ext,atm} - m_{ext,dust} + m_{zp} \quad (2)$$

$$d = \frac{1}{mas \cdot 0.001} \quad (3)$$

$$M_I = m_I - 5\log_{10}(d) + 5 \quad (4)$$

4.4 Creating Hertzsprung-Russell diagrams

Now we make our Hertzsprung-Russell diagrams. We selected the two filters for each source that gave us the most stars to compare. For M3 we took the blue and red filters with 2047 and 1947 stars respectively and for M67 we took the green and red filters with 127 and 136 stars respectively. We then subtracted the fluxes of the same stars between the images. We determined if two stars were the same if their centers were within 2.5 pixels of each other, which was half of the point spread function of the smallest objects detected.

5 Results and Analysis

Figure 3 is the Hertzsprung-Russell diagram for M3, presented with and without error bars so that the shape is easier to see. Each point represents one star with the y-axis being the absolute magnitude in the B filter and the x-axis being the difference in absolute magnitude between the B and R filters. This plot contains 1821 stars.

Similarly, figure 4 is the HR diagram for M67. The y-axis is the absolute magnitude in the V filter, and the x-axis is the difference between the absolute magnitudes of the V and R filters. This contains 123 stars.

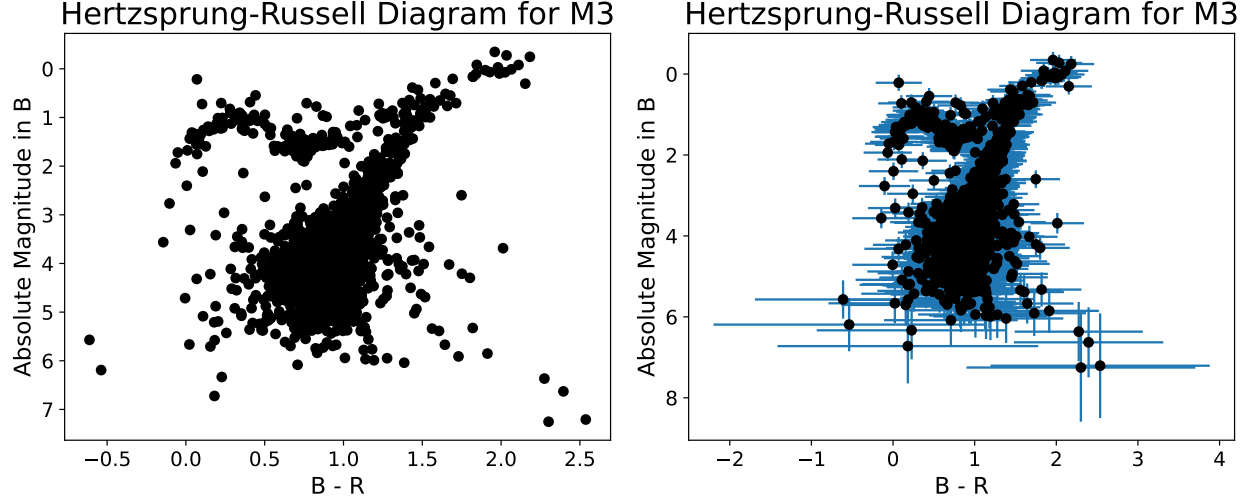


Figure 3: Our completed HR diagram for M3 with and without error bars. The y-axis is the absolute magnitude with the B filter and the x-axis is the difference of absolute magnitude between the B and R filters. These were chosen because we get the maximum amount of 1821 stars.

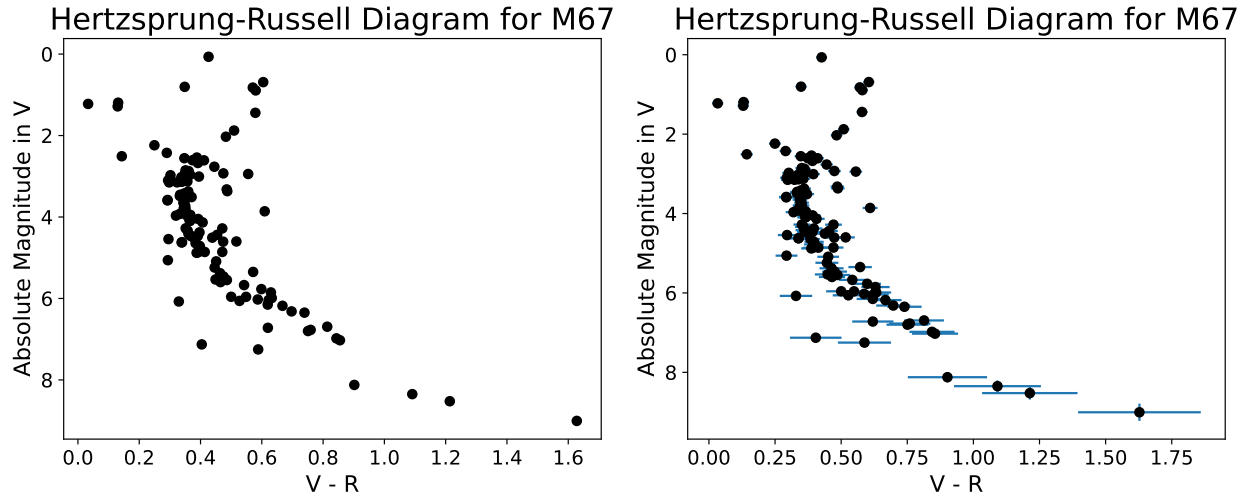


Figure 4: Our completed HR diagram for M67 with and without error bars. The y-axis is the absolute magnitude with the V filter and the x-axis is the difference of absolute magnitude between the V and R filters. These were chosen because we get the maximum amount of 123 stars.

The sources of errors are the apparent magnitude(σ_I) of PG 0918+029, the mili-arcsecond measurements(σ_{mas}) of all the sources, and the flux(σ_N) from source extractor. The propagated errors were then on the zero point magnitude($\sigma_{m_{zp}}$, equation 5), the apparent magnitude(σ_{m_I} , equation 6) of each source filter-combo, the distance of each source(σ_d , equation 7), the absolute magnitude(σ_{M_I} , equation 8) of each filter-source combo, which is the y-axis error in the HR diagrams, and the difference of filters, which is the x-axis error($\sigma_{\Delta m_I}$, equation 9) in the graphs.

$$\sigma_{m_{zp}} = \sqrt{\sigma_{m_I}^2 + \left(\frac{2.5\sigma_N}{N \cdot \ln(10)}\right)^2} \quad (5)$$

$$\sigma_{m_I} = \sqrt{\sigma_{m_{zp}}^2 + \left(\frac{2.5\sigma_N}{N \cdot \ln(10)}\right)^2} \quad (6)$$

$$\sigma_d = \frac{\sigma_{mas}}{mas^2 \cdot 0.001} \quad (7)$$

$$\sigma_{M_I} = \sqrt{\sigma_{m_I}^2 + \left(\frac{5\sigma_d}{d \cdot \ln(10)}\right)^2} \quad (8)$$

$$\sigma_{\Delta m_I} = \sqrt{\sigma_{M_{I1}}^2 + \sigma_{M_{I2}}^2} \quad (9)$$

6 Discussion

6.1 Fitting Isochrones

With these results, we can finally determine the age and metallicity of our clusters. This was done by overlaying isochrones of various ages and metallicities [14–23] and simply seeing which ones appeared to fit the best. We use Z for the metallicity parameter which is the percentage of elements heavier than helium that, in this case, the cluster has.

In figure 5 we show our best-fit isochrones corresponding to an ages between 11.22 Gyr and 15.85 Gyr and a Z of 0.001 [14–16]. The work done by VandenBerg et al. [24] found an age of 11.25 Gyr and a Z of 0.0003. Therefore, in figure 6 we also plot isochrones corresponding to ages between 10 Gyr and 14.13 Gyr and a Z of 0.0004 [14–16]. Unfortunately, the metallicity is not exact, but it is as close as we had access to in our time frame.

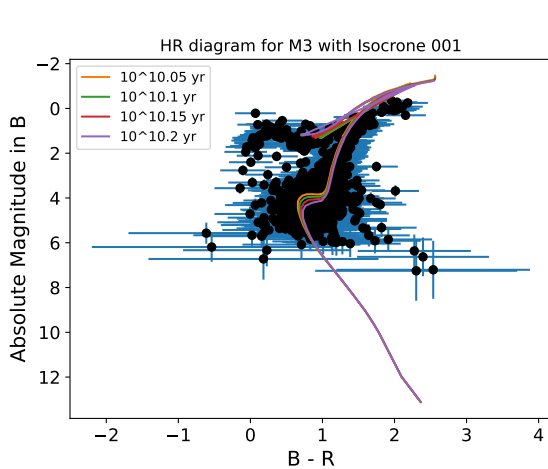


Figure 5: Our HR diagram with isochrones corresponding to ages between 11.22 Gyr and 15.85 Gyr and Z of 0.001 [14–16]. Based on the isochrones we tried, these ones provided the best fit by eye.

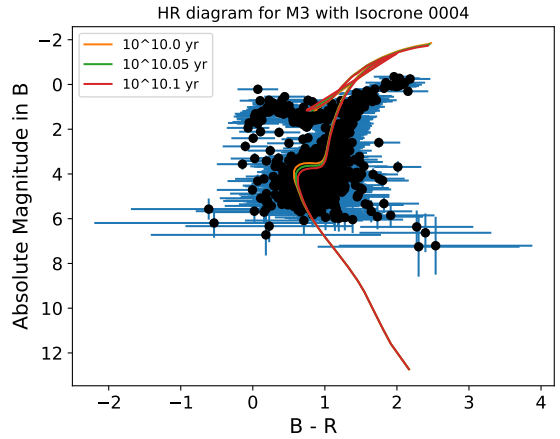


Figure 6: Our HR diagram with isochrones of ages between 10 Gyr and 14.13 Gyr and a Z of 0.0004 [14–16]. These isochrones are close to the properties that VandenBerg et al. [24] found for M3, so we plot them to see if our work agrees with theirs. Based on the fit mostly falling within the errors of ours, we do believe that our findings agree.

When comparing ours and VandenBerg et al.'s findings, we get overlapping age ranges, so we can agree on that. However, the metallicity that we found was approximately 3 times greater than what they observed.

Despite this, the lower metallicity isochrone still provides a close fit for all but the oldest stars, which makes sense because we expect younger stars to be high in metal content. Therefore, our results for M3 are within our tolerance for most of Vandenberg's results.

Similarly, we make the plots for M67. In this case, we found an age range of 3.55 Gyr to 4.49 Gyr and a Z of 0.019 [21]. Sarajedini et al. [4] suggests an age of 3.5-4 Gyr and Motta et al. [25] suggests a Z of 0.027. So, we plot isochrones with an age range of 2.82 Gyr to 4.49 and a Z of 0.03 [14-16]. Again, the metallicity is not ideal, but it is the closest one we could get in our time frame.

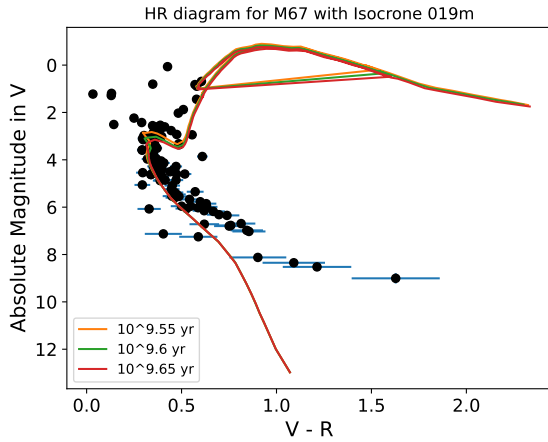


Figure 7: Our HR diagram with isochrones corresponding to ages between 3.55 Gyr to 4.49 Gyr and Z of 0.019 [21]. Based on the isochrones we tried, these ones provided the best fit by eye.

When comparing our fit with others' work, we again see that the age agrees well, but the metallicity is off. However, the 0.03 metallicity fit still provides a decent fit within our tolerance, so once again we obtain similar results to previous work.

For better results in future work, we could use a higher-resolution telescope to more accurately distinguish between stars and have a more thorough process for deciding which stars to use. The criteria we used to pick out "good" stars was quite arbitrary and may have cut out usable data while leaving some pairs or trios in one object. An improved method would try to eliminate all objects that aren't single stars without accidentally cutting out any single stars in the process.

6.2 Random Walks

Using random walk simulations we can gain insight into the path photons take when moving from the center of a star to its surface. For this example, we will use the Sun where photons travel approximately 0.5cm before being scattered in a random direction.

We start first in one dimension where we performed 1,000 walks of 10,000 steps each. Each step was randomly chosen to be +0.5cm or -0.5cm. The average displacement from this was -0.953cm and the RMS displacement was 51.1cm. This agrees with what we expect because a symmetrical random walk should be centered around 0cm which is where the average is. We plot the results in a histogram below to make this even clearer when we can see the Gaussian centered almost perfectly on 0cm and dropping off quickly at large displacements of ± 150 cm.

In three dimensions, we can use the approximation that the photon will travel $\frac{1}{\sqrt{3}}$ as far with each scatter. We then approximate the total number of steps with equation 10 and the total time with 11 where S_{tot} is the

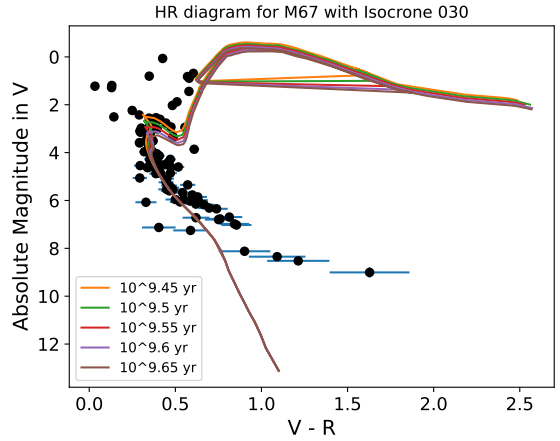


Figure 8: Our HR diagram with isochrones of ages between 2.82 Gyr to 4.49 and a Z of 0.03 [14-16]. These isochrones are close to the properties that Sarajedini et al. [4] and Motta et al. [25] found for M67, so we plot them to see if our work agrees with theirs. Based on the fit mostly falling within the errors of ours, we do believe that our findings agree.

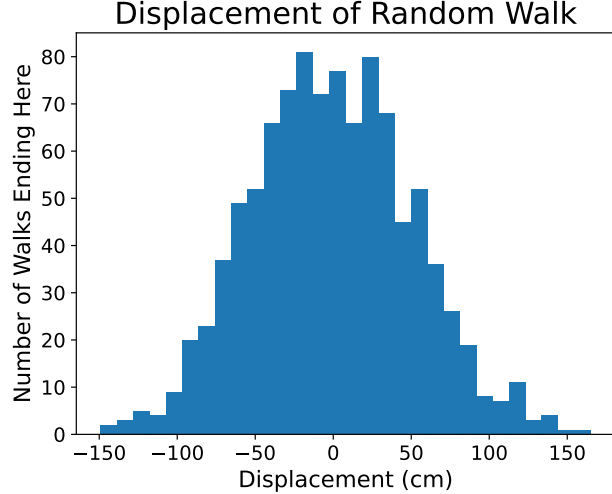


Figure 9: Displacement of 1,000 random walks of 10,000 steps and a step length of 0.5cm in either positive or negative x. As expected, we obtain a gaussian distribution around 0. The average displacement is -0.953cm and the RMS displacement is 51.1cm.

total number of steps, R_{Sun} is the radius of the Sun (69.634×10^9 cm), Δx_{ave} is the average displacement from the 1D walk, S_{1D} is the number of steps per walk in 1D, and c is the speed of light.

$$S_{tot} = \frac{R_{Sun}}{\Delta x_{ave}/\sqrt{3}} \cdot S_{1D} \quad (10)$$

$$t = \frac{S_{tot} \cdot 0.5}{c} \quad (11)$$

Plugging our numbers in we find this would take 1265 trillion steps which corresponds to 585 hours for a photon to escape from the center of the Sun. This is far less than the estimation of 170,000 years from Eddington [26]. The problem with our estimation is that in our calculations the photon is essentially still traveling in a straight path from the center to the surface of the sun, but just taking a step of $\frac{0.953}{\sqrt{3}}$ cm instead of a 0.5cm step. A better way to estimate this would be to take our random walk from 1D and convert it to 3D. Then let the simulation run until the photon escaped the sun. With an estimated time of 170,000 years and rearranging equation 11, however, this would take approximately 3.2×10^{21} steps which we do not have the time to test. Instead, I provide a 3D random walk with only one million steps to show how this would look. In figure 10, the photon started at the origin, in red, and ended 567.7cm from the origin, in orange, after traveling along the path in blue. The photon traveled a distance of 500,000cm only to displace 567.7cm compared to the Sun's 69.634×10^9 cm radius, giving a sense for why the timescale of this process is so large.

7 Conclusion

This study sought to determine the ages and metallicities of M3 and M67. After taking observations of these clusters we created an HR diagram for each and fit theoretical isochrones to them. Through this, we found M3 to be between 11.22 Gyr and 15.85 Gy and Z = 0.001, which agrees with previous observations, and M67 to be between 3.55 Gyr and 4.49 Gyr and Z = 0.019, which also agrees with other observations. In future work, we may improve our results by having a more rigid selection criterion of stars and access to a higher resolution telescope.

Random Walk of Photons in the Sun

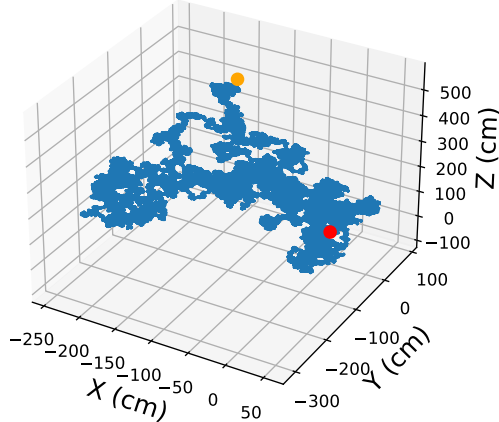


Figure 10: A one million step walk of step length 0.5cm in 3 dimensions. The red point is the starting location at the origin and the orange point is where it ended, 567.7cm away. This represents the path of a photon scattering from the center of the sun trying to reach the surface. Letting this run until it reaches the surface, 69.634×10^9 cm away, would require too much time, so we simply show the first million steps as an idea of what the walk looks like.

8 Acknowledgements

I would like to acknowledge my instructor Olivier Hervet, my teaching assistant Miguel Escobar Godoy, and my lab partners Atirath Dhara and JT Earwicker for their support on this project.

References

- [1] Eugene Vasiliev and Holger Baumgardt. Gaia EDR3 view on galactic globular clusters. , 505(4):5978–6002, August 2021.
- [2] A. et al. Sarajedini. An ACS Survey of Galactic Globular Clusters: M3 and its Stellar Population. *The Astrophysical Journal*, 667(1):L57–L60, 2007.
- [3] Gaia Collaboration. Gaia Data Release 2. Observational Hertzsprung-Russell diagrams. , 616:A10, August 2018.
- [4] Ata Sarajedini, Aaron Dotter, and Allison Kirkpatrick. Deep 2MASS Photometry of M67 and Calibration of the Main-Sequence J - K_S Color Difference as an Age Indicator. , 698(2):1872–1878, June 2009.
- [5] UCO/Lick Observatory. Nickel 40-inch reflector. <https://www.ucolick.org/public/telescopes/nickel.html>, Accessed May 2023.
- [6] Lick Observatory. Lick Observatory photometric filter curves, 2010.
- [7] Kyle Barbary. Source extractor photometry. <https://sep.readthedocs.io/en/v1.1.x/>, 2021.
- [8] Arlo U. Landolt. UBVRI Photometric Standard Stars in the Magnitude Range 11.5 \pm V \pm 16.0 Around the Celestial Equator. , 104:340, July 1992.
- [9] GALEXTIN. GALEXTIN official website. <http://www.galextin.org/>.

- [10] Eduardo B. Amôres, Ricardo M. Jesus, André Moitinho, Vladan Arsenijevic, Ronaldo S. Levenhagen, Douglas J. Marshall, Leandro O. Kerber, Roseli Künzel, and Rodrigo A. Moura. Galextin: an alternative online tool to determine the interstellar extinction in the milky way. *Monthly Notices of the Royal Astronomical Society*, 508(2):1788–1797, December 2021.
- [11] SIMBAD astronomical database. <http://simbad.u-strasbg.fr/simbad/>. Accessed on May 8, 2023.
- [12] Gaia Collaboration. VizieR Online Data Catalog: Gaia EDR3 (Gaia Collaboration, 2020). *VizieR Online Data Catalog*, page I/350, November 2020.
- [13] Provided by our instructor Olivier Hervet.
- [14] L. Girardi, G. Bertelli, A. Bressan, and C. Chiosi. Evolutionary tracks and isochrones for low- and intermediate-mass stars: From 0.15 to $7 M_{\odot}$, and from $Z=0.0004$ to 0.03. , 141:371–383, jun 2000.
- [15] G. Bertelli, A. Bressan, C. Chiosi, F. Fagotto, and E. Nasi. Evolutionary sequences of stellar models with new radiative opacities. IV. $Z=0.004$ and $Z=0.008$. , 106:275, nov 1994.
- [16] L. Girardi, G. Bertelli, C. Chiosi, and A. Bressan. Theoretical isochrones from models with new radiative opacities. , 117:113, apr 1996.
- [17] A. Bressan, F. Fagotto, G. Bertelli, and C. Chiosi. Stellar evolution tracks and isochrones with new radiative opacities. *Astronomy and Astrophysics Supplement Series*, 100:647, 1993.
- [18] F. Fagotto, A. Bressan, G. Bertelli, and C. Chiosi. Evolutionary sequences of stellar models with new radiative opacities. iii - $z = 0.02$. *Astronomy and Astrophysics Supplement Series*, 104:365, 1994.
- [19] F. Fagotto, A. Bressan, G. Bertelli, and C. Chiosi. Evolutionary sequences of stellar models with new radiative opacities. v - $z = 0.0004$ and $z = 0.05$. *Astronomy and Astrophysics Supplement Series*, 105:29, 1994.
- [20] L. Girardi. Personal communication. 2001.
- [21] P. Marigo, L. Girardi, and C. Chiosi. A new library of theoretical stellar population synthesis models. II. Stellar models and isochrones for intermediate and low mass stars with $[Fe/H] = -2.2$. , 371:152–167, 2001.
- [22] P. Marigo and L. Girardi. A new library of theoretical stellar population synthesis models. III. Models for mixed stellar populations. , 377:132–150, 2001.
- [23] B. Salasnich, L. Girardi, A. Weiss, and C. Chiosi. Population synthesis in the blue. IV. Accurate model predictions for Lick indices and UBV colors in single stellar populations. , 361:1023–1044, 2000.
- [24] Don A Vandenberg, K Brogaard, R Leaman, and L Casagrande. The ages of 55 globular clusters as determined using an improved δv_{TO}^{HB} method along with color–magnitude diagram constraints, and their implications for broader issues. *The Astrophysical Journal*, 775(2):134, 2013.
- [25] Clio Bertelli Motta, Maurizio Salaris, Anna Pasquali, and Eva K. Grebel. Observing the products of stellar evolution in the old open cluster M67 with APOGEE. *Monthly Notices of the Royal Astronomical Society*, 466(2):2161–2174, 03 2017.
- [26] Arthur Eddington. The internal constitution of the stars. *Philosophical Transactions of the Royal Society of London. Series A, Containing Papers of a Mathematical or Physical Character*, 226(893):659–713, 1926.